

Earth and Space Science



RESEARCH ARTICLE

10.1029/2023EA002840

Millennial-Scale Changes in Atmospheric Nitrous Oxide During the Holocene

Syed Azharuddin^{1,2}, Jinho Ahn^{1,3} , Yeongjun Ryu⁴, Ed Brook⁵, and Nasrin Salehnia^{1,3} 
¹School of Earth and Environmental Sciences, Seoul National University, Seoul, South Korea, ²Now at Graduate School of Environmental Studies, Nagoya University, Nagoya, Japan, ³Center for Cryospheric Sciences, Seoul National University, Siheung, South Korea, ⁴Department of Geosciences, Princeton University, Princeton, NJ, USA, ⁵College of Earth, Ocean & Atmospheric Sciences, Oregon State University, Corvallis, OR, USA

Key Points:

- High-resolution N₂O record from the South Pole Ice core covering the Holocene epoch is investigated for N₂O variation
- Insight into the key drivers of atmospheric N₂O on millennial time scales during the Holocene is provided
- N₂O exhibits two local maxima during 11.0–10.0 ka and 3.0–2.2 ka, and two local minima during 8.8–6.2 ka and at around 1.4 ka

Supporting Information:

Supporting Information may be found in the online version of this article.

Correspondence to:

J. Ahn,
jinhoahn@gmail.com

Citation:

Azharuddin, S., Ahn, J., Ryu, Y., Brook, E., & Salehnia, N. (2024). Millennial-scale changes in atmospheric nitrous oxide during the Holocene. *Earth and Space Science*, 11, e2023EA002840. <https://doi.org/10.1029/2023EA002840>

Received 17 JAN 2023
Accepted 15 AUG 2023

Author Contributions:

Conceptualization: Syed Azharuddin, Jinho Ahn, Yeongjun Ryu, Ed Brook
Data curation: Syed Azharuddin, Ed Brook, Nasrin Salehnia
Formal analysis: Syed Azharuddin
Funding acquisition: Jinho Ahn
Investigation: Syed Azharuddin, Jinho Ahn
Methodology: Syed Azharuddin, Ed Brook
Project administration: Jinho Ahn
Resources: Nasrin Salehnia
Software: Syed Azharuddin
Supervision: Jinho Ahn
Validation: Syed Azharuddin, Jinho Ahn
Visualization: Syed Azharuddin

Abstract Nitrous oxide (N₂O) is an important greenhouse gas which destroys the ozone in the stratosphere. Primary sources of atmospheric N₂O are nitrification and denitrification in terrestrial soils and the ocean, and the main sink is photolysis in the stratosphere. Studies have mostly focused on the climate-related response of N₂O during glacial-interglacial periods. However, its mechanism of variation during the Holocene remains unclear. We present a high-resolution N₂O record from the South Pole Ice (SPICE) core covering the Holocene epoch. The millennial-scale N₂O trend agrees with existing records. We constructed a Holocene composite consisting of the new N₂O measurements in SPICE and existing records from other ice core sites. The N₂O composite reveals four distinct periods of N₂O variation during 11.5–10.0 ka, 10.0–6.2 ka, 6.2–2.2 ka, and 2.2–1.4 ka, including two maxima in 11.0–10.0 ka and 3.0–2.2 ka and minima in 8.8–6.2 ka and approximately 1.4 ka. Apart from these, our new high-resolution record from SPICE shows a short-term N₂O decrease around 2.8 ka which is not observed in other records possibly due to lower sample resolution and/or higher age smoothing. Comparison of our new Holocene N₂O composite with the paleo-proxy records suggests the plausible linkage of major monsoon (Asian, North African, South and North American, and Australian-Indonesian monsoon) and upwelling (Arabian Sea and Eastern Tropical South Pacific) regions in regulating the atmospheric N₂O during the Holocene.

Plain Language Summary Nitrous oxide (N₂O) is an important greenhouse and ozone-depleting gas. The growing level of N₂O in the atmosphere is of global concern, and records of past N₂O variations can provide an essential context for understanding the links between N₂O and climate change. In this study, we report a new, high-quality N₂O record covering the Holocene epoch using an ice core obtained from the South Pole. Our record shows four important periods of N₂O variation during 11.5–10.0 ka, 10.0–6.2 ka, 6.2–2.2 ka, and 2.2–1.4 ka. These include two local N₂O maxima in 11.0–10.0 ka and 3.0–2.2 ka and minima in 8.8–6.2 ka and approximately 1.4 ka. Comparison with climate records suggests that the variation in monsoon precipitation and ocean productivity contributed to centennial- to millennial-scale N₂O variations during the Holocene.

1. Introduction

Nitrous oxide (N₂O) is a significant atmospheric greenhouse gas that responds to climate variation and is responsible for stratospheric ozone destruction (Prather et al., 2015). Anthropogenic emissions during industrialization have majorly contributed to the remarkable increase in atmospheric N₂O concentration from ~270 ppb in 1750 to ~332 ppb in early 2020 (Machida et al., 1995; Fluckiger et al., 2002; Rubino et al., 2019; N₂O hemispheric and global monthly mean from the ESRL/NOAA 2020). Recent estimates suggest an anthropogenic contribution of ~40% in the current total N₂O emission (IPCC AR6, 2021), whereas 60% of the emissions originate from natural sources. Terrestrial and oceanic sources account for ~60% and ~40% of N₂O emissions from the natural environment, respectively (Battaglia & Joos, 2018; Tian et al., 2020).

Variations in pre-industrial N₂O emissions from diverse sources are closely correlated with ecological processes regulating the cycling of nitrogen (N) and carbon (C) on land and in the ocean (Gruber & Galloway, 2008). N₂O production is contingent on metabolic processes (nitrification and denitrification) performed by specific groups of bacteria (Stehfest & Bouwman, 2006; Xu et al., 2017). Some hotspots of the globe, where major N₂O contributions from these processes occur include the terrestrial soils in the tropical forests and marine suboxic waters around the major upwelling regions overlying the oxygen minimum zones (OMZs) (Babbin et al., 2015; Cohen &

© 2024 The Authors.

This is an open access article under the terms of the [Creative Commons Attribution-NonCommercial License](#), which permits use, distribution and reproduction in any medium, provided the original work is properly cited and is not used for commercial purposes.

Writing – original draft:

Syed Azharuddin, Jinho Ahn,
Yeongjun Ryu, Ed Brook

Writing – review & editing:

Syed Azharuddin, Jinho Ahn,
Yeongjun Ryu, Ed Brook, Nasrin Salehnia

Gordon, 1979; Joos et al., 2020). The net N_2O produced during these processes depends on environmental conditions and production pathways (Joos et al., 2020). These conditions include temperature, water and oxygen levels, substrate availability etc. (Wang et al., 2018; Zhuang et al., 2012). The major terrestrial N_2O effluxes are associated with tropical areas, including Central and South America, Central Africa, and Southeast Asia (Xu et al., 2017). In such areas, denitrification is predominant in producing N_2O , with limited contribution from nitrification under low oxygen conditions in soils (Joos et al., 2020).

On the other hand, primary sites for marine N_2O emissions occur in coastal upwelling systems around major OMZs (Agnihotri et al., 2006; Naqvi & Noronha, 1991). In the productive regions, microbial respiration during the decomposition of organic matter leads to the formation of anoxic waters (less than 10 nmol L^{-1} of O_2), also known as oxygen-deficient zones (ODZs) (Tiano et al., 2014). These ODZs are surrounded by a large volume of hypoxic waters (below $20 \text{ } \mu\text{mol L}^{-1}$ of O_2), which accelerates denitrification at the core of the anoxic zone and nitrification at the oxic-anoxic interface, making OMZs one of the significant sources of N_2O (Babbin et al., 2015; Ji et al., 2015).

The primary sinks for N_2O are the stratospheric photolysis of N_2O by ultraviolet light and its chemical reaction with excited oxygen (Minschwaner et al., 1998). N_2O has a relatively long atmospheric lifetime (approximately 123 ± 10 years) and therefore mixes effectively in the troposphere, reflecting similar values globally for a particular time (Prather et al., 2015). Hence, the N_2O concentration retrieved from the ice cores can be a potential proxy for studying variations in the global nitrogen cycle.

During the last few decades, several detailed ice core N_2O records covering different aspects have been established (Fischer et al., 2019; Flückiger et al., 2002, 2004; Schilt et al., 2010, 2013; Spahni et al., 2005). These include the glacial-interglacial N_2O variability and millennial-scale N_2O variations since the last glacial period, with a focus on N_2O response to abrupt climate events (Fischer et al., 2019; Flückiger et al., 1999, 2002; Schilt et al., 2010, 2013; Spahni et al., 2005). On a glacial-interglacial timescale, concentrations of N_2O fluctuate between 280 and 180 ppb during warm and cold periods, respectively (Schilt et al., 2013). These climate variations have also been associated with changes in the Atlantic meridional overturning circulation (AMOC) (Henry et al., 2016; Pedro et al., 2018). The weakening of the AMOC causes a shift in the Intertropical Convergence Zone (ITCZ) southward, leading to the weakening of tropical monsoon precipitation (Wang et al., 2007) as well as the variation in OMZ strength around the Arabian Sea and Pacific Ocean (Pichevin et al., 2007; Schmittner et al., 2007). Hence, rapid climate change (warming/cooling) is believed to affect both terrestrial and marine sources of N_2O production (Pichevin et al., 2007; Schmittner et al., 2007). Flückiger et al. (2002) focused on the N_2O variation during the entire Holocene and reported a local N_2O minimum at $\sim 8 \text{ ka}$ (thousand years before present or ka where the present is 1950 CE). The study also suggested that the N_2O record is more similar to the CO_2 record than the CH_4 record during the Holocene. Ryu et al. (2020) studied the high-resolution N_2O records for the last two millennia and reported a pronounced N_2O minimum at $\sim 600 \text{ CE}$ ($\sim 1.4 \text{ ka}$) coeval with the reorganization of tropical hydroclimate and changes in ocean productivity. However, the detailed feedback mechanism responsible for the N_2O -climate relationship and its interdependence with terrestrial and marine processes during the entire Holocene remains elusive owing to the lack of high-resolution N_2O records covering the Holocene.

We present a new high-resolution N_2O record from the South Pole Ice (SPICE) core during the last ~ 11 thousand years. Additionally, a composite N_2O record is constructed by combining the new measurements from SPICE with the existing records from other ice cores. The results provide insight into the key drivers of atmospheric N_2O on millennial time scales during the Holocene.

2. Materials and Methods

2.1. Site Description

The SP14 core site is located near the geographical South Pole (89.99°S , 98.16°W) at a surface elevation of 2,835 m. The ice accumulation rate around the SPICE site is 8 cm water-equivalent per year or w.e./yr (Lilien et al., 2018; Mosley-Thompson et al., 1999), and the annual mean temperature measured in the firn is -51°C (Severinghaus et al., 2001). Under modern climatological conditions, the estimated age spread of enclosed air for the SPICE site (calculated by the width of the age distribution curve at half height) is around 65 years (Battle et al., 1996; Buizert, 2012). The age difference between trapped bubbles (gas age) and surrounding ice

(ice age) is referred to as the Δ age (Bender et al., 2006). The Holocene value of Δ age for the SPICE site is $\sim 1000 \pm 50$ years, calculated by a firm densification model and empirical matching of CH_4 gas chronology (Epifanio et al., 2020).

2.2. N_2O Measurement

We applied a high-precision wet extraction (double melt-refreeze) method for SPICE ice, as Ryu et al. (2018) described. We used 17–18 g of ice for each measurement. The ice cutting was performed in a walk-in freezer maintained at approximately -20°C . The trimmed ice pieces were placed in specially designed glass flasks and bolted on a flat flange with a copper gasket for sealing under a high vacuum while attached to the vacuum extraction line. Laboratory-made bubble-free high-purity ice was also used for blank correction. The glass sample cups were initially submerged in a pre-chilled ethanol bath (-75°C) and evacuated for approximately 50 min to remove the ambient air in the flask and any contaminants on the ice surface. After evacuation, the ice pieces were melted to liberate the enclosed air and collected in the headspace of each sample flask. Subsequently, the meltwater was refrozen before analysis. The concentration of N_2O in the liberated air in the headspace of each sample flask was measured using an Agilent 7890b gas chromatograph (GC) equipped with a micro-electron capture detector. We analyzed standard air with an N_2O concentration of 265 ppb from the National Oceanic and Atmosphere Administration (NOAA) before and after the sample measurement. Due to the high solubility of N_2O in water, we repeated the N_2O measurement during the second melt-refreeze cycle, which corrected $\sim 3\%$ (6–8 ppb) of the total N_2O concentration. Therefore, high-precision wet extraction (double melt-refreeze) is an accurate method to obtain the precise N_2O concentration in ice core samples, which would otherwise result in 6–8 ppb lower concentrations with a single melt-refreeze cycle (Ryu et al., 2018). A total of 177 sample depths with at least two horizontal replicates were measured. The inter-day precision during the N_2O measurement was determined by measuring more replicates (three or four) from 19 depths and calculating their pooled standard deviation. Further, to calculate the overall N_2O precision in the SPICE core, including ice quality and experimental uncertainty, we selected long ice pieces (~ 20 cm each) from five different depths. Eight continuous measurements were done (at ~ 2 cm intervals) from each of the five long ice pieces ($n = 40$) (Table S1 in Supporting Information S1). The obtained raw N_2O values were corrected for gravitational correction using the average $\delta^{15}\text{N}$ of N_2 of the SPICE core during the Holocene (0.539 ‰) and the following equation:

$$\text{N}_2\text{O}_{\text{corrected}} = \text{N}_2\text{O}_{\text{measured}} \left(1 - \Delta M \frac{\delta^{15}\text{N}}{1000} \right)$$

where $\Delta M = 15.05$ g/mol which refers to the difference between the masses of air (28.96 g/mol) and mass of N_2O (44.013 g/mol). The gravitational correction decreased the final N_2O concentration by ~ 2.5 ppb. The average analytical uncertainty for repeated measurements in SPICE is 1.3 ppb which is better than the uncertainties reported in previous studies ranging between 2.5 and 3.6 ppb (Figure 1).

2.3. N_2O Composite

We prepared a composite N_2O record of the Holocene using our results from SPICE samples measured at 177 different depths and existing records from EPICA Dome C (EDC), Dronning Maud Land (EDML) (Flückiger et al., 2002; Schilt et al., 2010), Talos Dome Ice (TALDICE), North Greenland Ice Core Project (NGRIP) (Fischer et al., 2019), Law Dome (Rubino et al., 2019) and Styx and NEEM (Ryu et al., 2020) ice cores. The modern records of N_2O concentrations from atmospheric monitoring show an interhemispheric gradient of ~ 0.8 ppb and it is likely to be smaller during pre-industrial time due to higher anthropogenic emissions in the Northern Hemisphere (Ishijima et al., 2009), which is well within the individual analytical uncertainties of each ice core record. Therefore, N_2O records from Antarctic and Greenland ice cores were used without further inter-hemispheric correction in preparing the Holocene N_2O composite. A correction for gravitational fractionation based on the average $\delta^{15}\text{N}$ of N_2 at each ice core site was also applied to the other ice core records except Law Dome, which is already corrected (Rubino et al., 2019). The N_2O record from each ice core was synchronized to the common WD2014 age scale (Sigl et al., 2016; See Supporting Information S1 for more details). For each record, the N_2O concentration is interpolated to get the yearly-resolved N_2O curves before constructing a composite N_2O curve. We used the Monte Carlo average (MCA) method with a 250-year running average to understand the millennial-

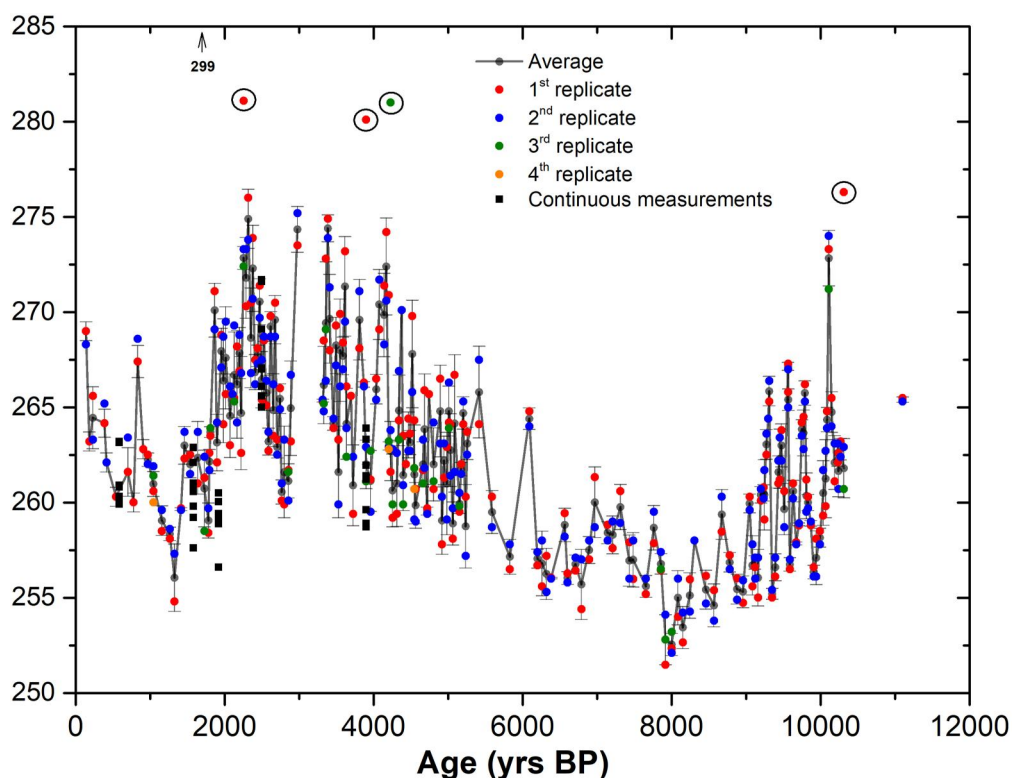


Figure 1. N_2O concentrations measured in the South Pole Ice Core during the Holocene. The replicate measurements for each depth are indicated in different colored symbols (first replicate–red, second replicate–blue, third replicate–green, fourth replicate–yellow). Dark gray symbols indicate the average N_2O concentration at each depth. Error bars indicate the uncertainty of replicated measurements. The black squares indicate the continuous measurements in long ice pieces. The black-circled values are the outliers identified using the Grubbs test (Grubbs, 1969). Refer text for more details.

scale changes in atmospheric N_2O during the Holocene. The uncertainty associated with the MCA record was implemented by repeating the MCA algorithm 10,000 times (Figure 2 and Figure S1 in Supporting Information S1). See Supporting Information S1 for more details on the MCA and uncertainty calculations.

2.4. Total Flux Calculations

N_2O emissions were estimated by calculating the total N_2O flux from the N_2O composite using a two-box model (Figure S2 in Supporting Information S1). The box model of Schilt et al. (2014) was modified using the method by Ryu et al. (2020) to calculate the total N_2O flux without using the N_2O isotopologues ($\delta^{15}\text{N}$ and $\delta^{18}\text{O}$ of N_2O). Due to the lack of isotope data, we could not distinguish the N_2O fluxes from terrestrial and marine sources. The model assumed the stratosphere and troposphere as individual boxes where the stratospheric N_2O destruction and troposphere-stratosphere N_2O exchange were well constrained. The model used the tropospheric N_2O lifetime of 123 ± 10 years (Prather et al., 2015) and the stratosphere-troposphere mass exchange rate of $5.37 \pm 0.26 \times 10^{17} \text{ kg yr}^{-1}$ (Ishijima et al., 2007) with a 250 yr cut-off period (COP). Each run was executed by random propagation within the uncertainty range of N_2O concentration, N_2O lifetime, and stratosphere-troposphere exchange rate using the Monte Carlo approach across all the possibilities ($n = 10,000$). We also performed a sensitivity test of our 2-box model for different N_2O lifetimes and stratosphere-troposphere exchange rates fixed at the maximum, minimum and average values. Initially, we fixed the N_2O lifetimes to 133, 123 and 113 (std dev = 0) and performed runs for each scenario. We observed a significant increase of $\pm 0.85 \text{ TgN/yr}$ in the total N_2O flux with a decrease of 10 yrs in the N_2O lifetime which is similar to the 1 sigma uncertainty of our results of total N_2O flux. We also performed a similar test with the S-T exchange rate for three scenarios by fixing the values to the maximum ($5.63 \times 10^{17} \text{ kg yr}^{-1}$), minimum ($5.11 \times 10^{17} \text{ kg yr}^{-1}$) and average ($5.37 \times 10^{17} \text{ kg yr}^{-1}$). The results indicate a significant change in

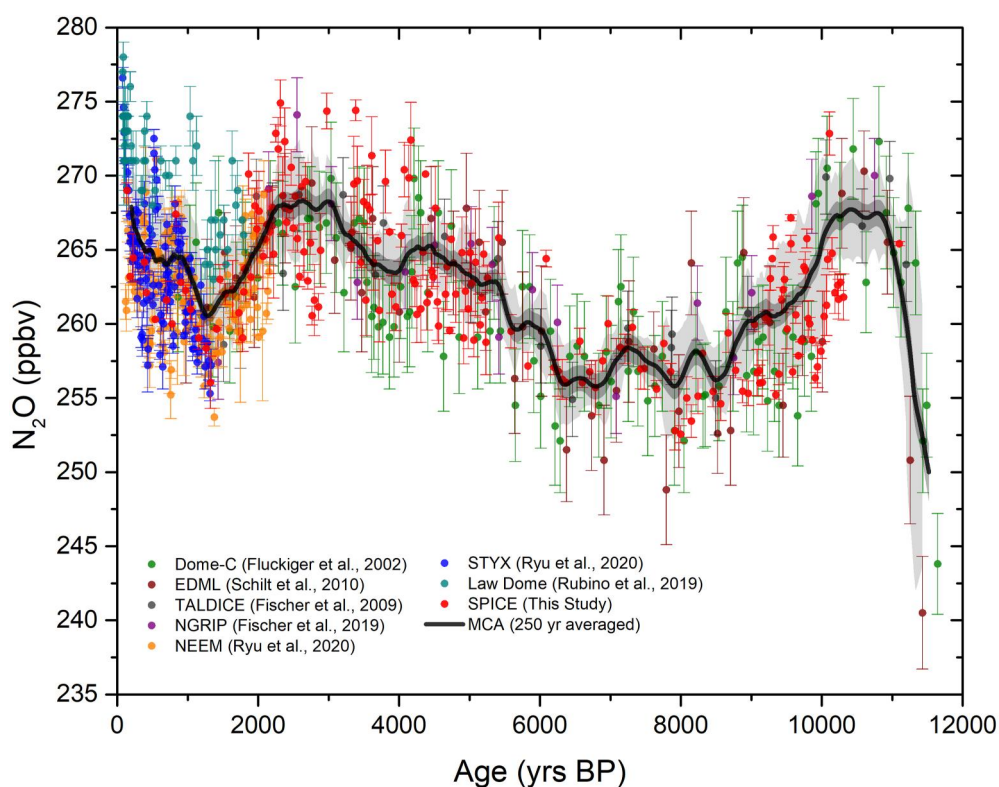


Figure 2. Compilation of new (SPICE) and existing N_2O records from EPICA Dome C (EDC) (Flückiger et al., 2002); Droning Maud land (EDML) (Schilt et al., 2010); Talos Dome Ice (TALDICE) and North Greenland Icesheet Project (NGRIP) (Fischer et al., 2019), Styx and NEEM (Ryu et al., 2020) and Law Dome (Rubino et al., 2019) ice core records during the pre-industrial Holocene. The solid line represents the Monte Carlo running average for 250 years. The dark gray shaded envelope represents the 1σ uncertainty in Monte Carlo Averaging, light gray shading indicates the 1σ uncertainty related to average N_2O from different records interpolated at each year.

N_2O flux ($\pm 0.04 \text{ TgN/yr}$) between the maximum and minimum values of the S-T exchange rate used in the model (Figure S3 in Supporting Information S1).

3. Data Quality

The SPICE site has a fairly low ice accumulation rate of $\sim 8 \text{ cm w.e./yr}$, resulting in relatively high smoothing in the gas record owing to gas diffusion and gradual bubble close-off processes in the firn column. The CH_4 age-distribution curve for the firn densification model of the SPICE site suggests a width of approximately 65 years at half height (Battle et al., 1996; Buizert, 2012). Hence, any abrupt change in N_2O from its preceding or successive value within 65 years may be considered an outlier, as these would not be representative of the actual atmospheric signals. Such outliers may arise owing to chemical interactions or microbial processes (Fischer et al., 2019; Flückiger et al., 2002), and experimental errors arising from contamination during ice trimming and/or drift due to background sensitivity of the GC experiments (Ryu et al., 2018). To overcome the GC drift, we repeated the measurement using replicated ice samples from each depth after a few weeks and averaged for the final N_2O concentration (Figure 1). The average standard deviation for replicate measurements was 1.3 ppb. The intra-day precision was calculated by averaging the pooled standard deviation of daily blank ice measurements, which is 1.8 ppb. The outliers in the multiple N_2O measurements at five depths were statistically rejected using the Grubbs test (Grubbs, 1969). The pooled standard deviation for samples measured three or more times on different days was 1.8 ppb ($n = 41$). On the other hand, the pooled standard deviation of continuous measurement of long ice pieces (at 2 cm intervals) was 2.5 ppb. Furthermore, the measured N_2O in the SPICE core over the last 2,200 years was compared with the high-resolution N_2O records of Styx and NEEM ice cores (Ryu et al., 2020) (Figure S4 in Supporting Information S1); which demonstrates consistency

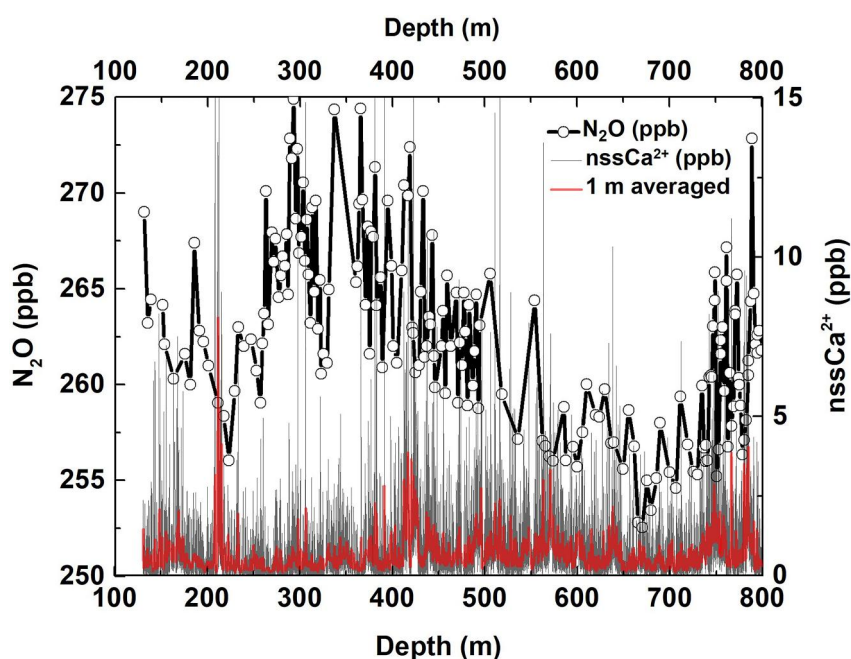


Figure 3. Comparison of N_2O (ppb) with nssCa^{2+} (ppb) variation (Winski et al., 2019) at depth scale in the SPICE core. Also, refer to Figure S5 in Supporting Information S1 for zoomed N_2O - nssCa^{2+} comparison during high N_2O fluctuation periods.

with the Styx and NEEM records measured in the same facility a few years prior (for the overlapping time periods) (Figure S4 in Supporting Information S1). These observations suggest new SPICE N_2O record determined herein is reliable.

A well-known concern for ice core N_2O data is the possibility of in situ production of N_2O (Flückiger et al., 2002; Schilt et al., 2010). The in situ N_2O production could result from biotic and abiotic origins (Rohde et al., 2008; Samarkin et al., 2010). The microbes in ice may oxidize NH_4^+ (substrate) to nitrate (nitrification) or reduce nitrate to nitrogen gas (denitrification) and produce N_2O as an in situ intermediate product (Phillippot et al., 2007; Röthlisberger et al., 2000; Sowers, 2001). Such N_2O production may contribute to high N_2O concentrations observed at specific depths depending on the concentration of impurities that facilitate the in-situ processes. This raises an important question as to whether all the N_2O data measured in the SPICE core covering the Holocene represent the atmospheric concentration or if some of them are elevated owing to in situ N_2O production. In general, ice from warmer periods, such as the Holocene, is expected to be least affected by impurities that are carried by the dust deposited with snow (Fischer et al., 2019; Flückiger et al., 2002). This is due to the higher dust deposition during glacial than interglacial periods (Schilt et al., 2010). It is worth noting that the ice in Greenland typically contains higher levels of dust than the ice found in Antarctica. (Flückiger et al., 2002; Lee et al., 2020). To assess these possibilities, we compared our N_2O data with high-resolution non-sea-salt calcium (nssCa^{2+}) concentrations (Winski et al., 2019) (Figure 3 and Figure S5 in Supporting Information S1).

nssCa^{2+} is an indicator of dust content in ice, which may indirectly correspond to the microbial content in the ice samples (Röthlisberger et al., 2000). The fluctuations in high-resolution N_2O data did not significantly correlate with the cm-scale changes in the nssCa^{2+} record (see Figure S6 in Supporting Information S1). These observations suggest that the Holocene N_2O record of the SPICE core may not be affected by Ca (dust)-related in-situ N_2O production. Overall, the new N_2O measurements presented here have good reproducibility during replicate measurements. On the other hand, the continuous measurement of long ice pieces (2 cm interval) also shows a similar reproducibility at four out of five depths (Table S1 in Supporting Information S1). Considering the 65-yr width of the gas age distribution curve and accumulation rate (8 cm/yr) at the SPICE site, eight pieces used in continuous measurement should represent ~ 2 yr age, which should ideally have a similar N_2O concentration. However, one of the depth intervals (305 m) shows higher variation within 20 cm unrelated to Ca (dust), possibly due to an additional factor that increases the observed variability on these short time intervals.

4. Results

Here, using SPICE, we extend the high-resolution N_2O record further to cover the last 11 ka (Figure 1). The N_2O data from the SPICE core are consistent with existing records on millennial timescales and reveal new details on the multi-centennial scale. The SPICE N_2O concentration shows a variation of 20 ppb between 11 and 8 ka, with a maximum of 273 ppb and a minimum of 253 ppb. From 8.0 ka to 3.3 ka, there was a gradual increase of 21 ppb in SPICE N_2O concentration, with a maximum of 274 ppb and a minimum of 253 ppb. Following this, there was a sudden drop of 15 ppb in SPICE N_2O concentration centering around 2.8 ka. Between 2.8 and 2.2 ka, the N_2O concentration at the SPICE site rose by 15 ppb, followed by an 18 ppb decrease between 2.2 ka and 1.4 ka. The N_2O minima (at 8.0 ka and 1.4 ka) and maximum at 2.2 ka observed in our high-resolution data from the SPICE site are also observed in other ice core records such as EDC, EDML, TALDICE, and NGRIP (Fischer et al., 2019; Flückiger et al., 2002; Schilt et al., 2010) (Figure 2). However, the N_2O minimum at 2.8 ka is not observed in the existing low-resolution records from other ice core sites. The maximum available data points between 2.5 and 3.0 ka are from SPICE which shows a significant drop in N_2O concentration around 2.8 ka. The MCA curve of SPICE-only data between 3.5 and 1.0 ka shows a prominent 8 ppb ($\sim 0.5 \text{ TgNyr}^{-1}$) decrease around 2.8 ka (Figure S1 in Supporting Information S1). On the other hand, the N_2O record of Dome-C does not show any change in concentration around 2.8 ka, possibly due to higher smoothing and wider age distribution at Dome-C than at the SPICE site. This means that there could be several multi-centennial atmospheric signals that may be observed only in ice core records of lower age smoothing (e.g., Styx, NEEM, Law Dome or even SPICE) but may not be archived in EDC, even in the higher sample resolution records. Hence, the short-term N_2O drop in SPICE at around 2.8 ka may likely represent a true atmospheric signal which is not captured in other N_2O records possibly due to lower sample resolution and/or higher age smoothing.

We prepared an MCA N_2O composite to cover the entire Holocene (considering the sample gaps in our new SPICE record) by compiling our new N_2O results with the available records from EDC, EDML, TALDICE, Styx, NEEM, Law Dome, and NGRIP ice core (Law Dome, Styx, and NEEM cover only last ~ 2 ka) averaged at 250 years (Figure 2). The main distinctive features of the Holocene N_2O variations observed in our N_2O composite include two N_2O maxima at approximately 11–10 ka and 3–2.2 ka, followed by minima at approximately 8–6 ka and ~ 1.4 ka, respectively. These millennial-scale features observed in our new N_2O composite agree well with the N_2O composite record of Fischer et al. (2019). With the addition of new high-resolution N_2O measurements from SPICE, Styx and NEEM sites, our new MCA composite shows 2–3 ppb lower N_2O values as compared to the MCA composite of Fischer et al. (2019) (Figure S7 in Supporting Information S1). Overall, we observe a range of ~ 15 ppb in N_2O during the Holocene, along with four distinct periods of N_2O change during 11.5–10.0 ka, 10.0–6.2 ka, 6.2–2.2 ka, and 2.2–1.4 ka. The most considerable N_2O variation corresponds to the beginning of the Holocene (between 11.5 and 11.0 ka), where we observed an abrupt ~ 15 ppb increase in atmospheric N_2O based on mainly previous published records (Fischer et al., 2019; Schilt et al., 2014), which corresponds to a $\sim 0.8 \text{ TgNyr}^{-1}$ increase in total N_2O flux within 500 years assuming no change in N_2O lifetime (Figure S3 in Supporting Information S1). The main cause was attributed to the resumption of the Atlantic meridional overturning circulation (AMOC) during the Preboreal Oscillation (PB) (Henry et al., 2016; Pedro et al., 2018).

The composite record shows a noticeable decrease of ~ 10 ppb during 10.0–8.8 ka corresponding to a decrease of $\sim 0.5 \text{ TgNyr}^{-1}$ in total N_2O flux (Figure S2 in Supporting Information S1), which was followed by a prolonged N_2O minimum between 8.8 and 6.2 ka. Thereafter, the record shows a progressive increase in atmospheric N_2O concentration (~ 12 ppb) corresponding to a $\sim 0.5 \text{ TgNyr}^{-1}$ increase in total N_2O flux between 6.2 and 3.0 ka. Finally, the N_2O record shows another maximum at 3.0–2.2 ka, followed by a decrease over the next ~ 800 yrs to attain a minimum at around 1.4 ka. The 1.4 ka local N_2O minimum was also reported by a recent N_2O study from Styx, NEEM, and Law Dome ice core sites (MacFarling Meure et al., 2006; Rubino et al., 2019; Ryu et al., 2020). Subsequently, the pre-industrial increase of N_2O after 1.4 ka might be related to the increased agricultural activities (Syakila & Kroeze, 2011; Xu et al., 2017). Overall, the new SPICE record, combined with the existing records shows new features of N_2O variations on millennial time scales during the Holocene.

5. Discussion

The Holocene variation of all the three major greenhouse gases CO_2 , CH_4 , and N_2O provides interesting information about the regional climate variation influencing their production and emission from major source areas

(Flückiger et al., 2002). It is estimated that the ocean has been a dominant CO₂ source, whereas the terrestrial regions have been a net carbon sink during the Holocene (Brovkin et al., 2019; Goodwin et al., 2011). On the other hand, early and middle Holocene changes in atmospheric methane are related to the changes in Northern tropical wetlands (Yang et al., 2017; Zheng et al., 2014), whereas the late Holocene increase in atmospheric CH₄ is linked with the increase in orbitally controlled tropical sources, particularly in the Southern Hemisphere (Beck et al., 2018; Singarayer et al., 2011). However, the atmospheric N₂O variation during the Holocene is attributed to changes in both land and ocean N₂O sources (Flückiger et al., 2002). Our new Holocene N₂O composite shows two distinct N₂O maxima around PB (11–10 ka) and 3–2.2 ka, followed by successive minima at 8.8–6.2 ka and around 1.4 ka, respectively. N₂O production and emission in terrestrial environments primarily depend on temperature and precipitation changes that alter soil texture and moisture content (Liu et al., 2015), microbial ecology (Zhang et al., 2013), and substrate availability (Bai et al., 2013). In general, increased temperature and precipitation enhance N₂O emissions from soils (Bouwman et al., 2002; Potter et al., 1996). The main terrestrial N₂O source is the Tropical Forest and the precipitation changes during the monsoon season are suggested to be the important factor which influences the N₂O variability in these regions (Stehfest & Bouwman, 2006; Xu et al., 2017). On the other hand, marine N₂O production in oxic waters is dominated by nitrification (Battaglia & Joos, 2018), whereas the denitrification process dominates surrounding OMZ regions with a limited contribution from nitrification (Frey et al., 2020; Ji et al., 2015). The highest marine N₂O production and efflux are concentrated around sub-oxic waters with high productivity (Cohen & Gordon, 1978; Suntharalingam et al., 2000). The expansion of hypoxia in the water column during intensified OMZ causes an increase in marine production and outgassing of N₂O (Babbin et al., 2015; Ji et al., 2015; Naqvi et al., 2000). It is estimated that the majority of marine N₂O emissions come from regions where highly productive waters overlay shallow OMZs, such as the Eastern Tropical South Pacific (ETSP) and the Arabian Sea (AS) (Arevalo-Martinez et al., 2015; Yang et al., 2020). Therefore, to investigate further, we compared our N₂O composite with individual paleo-proxies of tropical precipitation and temperature as well as the marine oxygen minimum zone to understand the processes that occurred during the Holocene concerning the change in terrestrial and marine N₂O sources, respectively (Figures 4 and 5). Further, we conducted a correlation test by analyzing correlation coefficients between the N₂O composite and the paleo-proxy records from the vital regions for each period with the possible lead/lag times (Table 1). To establish correlations on land, we compared the speleothem records of oxygen isotope ($\delta^{18}\text{O}$), which serves as a proxy for past rainfall in major monsoon regions. For marine correlations, we examined the records of nitrogen isotope ratios ($\delta^{15}\text{N}$) in marine sediments, which is a good indicator of the subsurface denitrification process around oxygen minimum zones. Such correlations are not necessarily a causal connection throughout the Holocene but may give an idea about the plausible N₂O source during the important periods of N₂O variation discussed in this study.

5.1. 11.5–10.0 ka

The composite record shows a significant N₂O increase of ~15 ppb (~0.8 TgNyr⁻¹) during 11.5–11 ka followed by an N₂O maximum between 11 and 10 ka (Figure 2 & Figure S2 in Supporting Information S1). Looking at the air temperature record from South China, which is known for its high N₂O production, it is evident that there was a significant increase in temperature between 11.5 and 10.0 ka (Shi et al., 2021) (Figure 4). Following this increase, there was a decreasing trend after 10 ka. Further, we compared the oxygen isotope ($\delta^{18}\text{O}$) record of speleothem (a proxy for the past monsoon rainfall) from major monsoon regions with our N₂O composite. The $\delta^{18}\text{O}$ signatures of calcite are controlled by the seepage water in the caves, which preserves the records of past precipitation such that the increase in precipitation is reflected by a negative excursion in $\delta^{18}\text{O}$. The Asian Monsoon speleothem records from Dongge Cave suggest an intensification of the Asian Monsoon between 11.5 and 10.0 ka, which is followed by a declining Asian Monsoon trend during the Middle and Late Holocene (Dykoski et al., 2005) (Figure 4). On the other hand, the monsoon records of other regions show variable patterns during each of the periods. Furthermore, the correlation test indicates a good correlation of N₂O trend with Asian (Dongge Cave), N. American (Pink Panther), N. African (Soreq Cave) and Indonesian-Australian Monsoon (Liang Luar Cave) regions (Asmerom et al., 2007; Bar-Matthews & Ayalon, 2011; Dykoski et al., 2005; Griffiths et al., 2009). These observations are in agreement with the N₂O isotope-based terrestrial flux (F_{land}) record of Fischer et al. (2019) showing ~0.3 TgNyr⁻¹ increase in terrestrial N₂O emission between 11.5 and 10 ka (Figure 4).

Looking at marine records, we compared the N₂O composite with the $\delta^{15}\text{N}$ signatures in marine sediments from major oxygen minimum zones (ETSP and AS) (Figure 5). The $\delta^{15}\text{N}$ record from both AS (RC-27-23 and

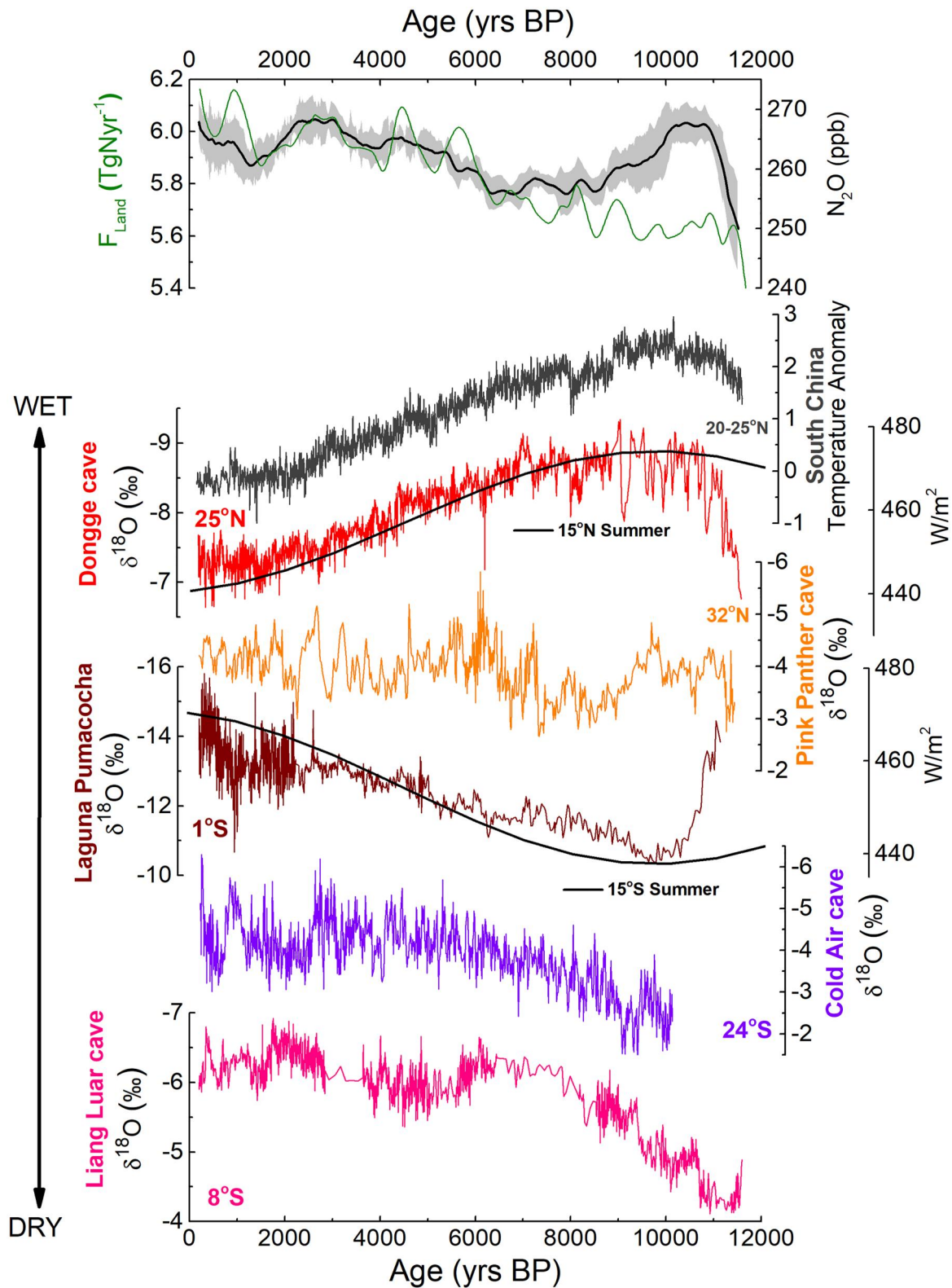


Figure 4.

RC-27-14) and ETSP (GeoB7139-2 and M772-03-2) exhibits enriched values, indicating strong OMZ conditions, which reflect higher N_2O emissions from these regions between 11.5 and 10.0 ka (Altabet et al., 2002; De-Pol-Holz et al., 2007; Mollier-Vogel et al., 2019) (Figure 5). These observations are also reflected in the correlation analysis results showing a highly correlated N_2O composite and $\delta^{15}\text{N}$ of bulk sediment around the Chile Margin (Site GeoB7139-2), Peru Margin (Site M772-03-02), and AS (Site RC-27-23) indicating high N_2O emission from these regions (Table 1). At the same time, the N_2O isotope-based ocean flux (F_{ocean}) shows a notable $\sim 0.6 \text{ TgNyr}^{-1}$ increase in marine N_2O emission (Fischer et al., 2019) (Figure 5). These observations suggest that the rise in atmospheric N_2O concentration between 11.5 and 10.0 ka was caused by the increased emissions from both terrestrial and marine N_2O sources.

5.2. 10.0–6.2 ka

The N_2O composite shows a prominent $\sim 10 \text{ ppb}$ ($\sim 0.5 \text{ TgNyr}^{-1}$) decrease between 10.0 and 8.8 ka which was followed by a prolonged N_2O minimum between 8.8 and 6.2 ka. These trends are similar to the early-mid-Holocene decrease in atmospheric CH_4 , attributed to the decline in Northern and Southern Hemisphere emissions during the early and mid-Holocene respectively (Beck et al., 2018). During the same period (between 10.0 and 6.2 ka), the Asian and N. African monsoons show insignificant correlation ($|r| < 0.3$) with the N_2O trend whereas the N. American Monsoon shows a weak correlation (Table 1). On the other hand, the Southern Hemisphere monsoon shows intensification during the N_2O decrease. Looking at the marine records, $\delta^{15}\text{N}$ -proxy records from both the Arabian Sea and ETSP show a contemporaneous decrease by 2–4‰, indicating a large-scale weakening of OMZs related to the deepening of oxycline in those regions (Agnihotri et al., 2006; Altabet et al., 2002; De-Pol-Holz et al., 2007; Mollier-Vogel et al., 2019). Such prominent weakening of OMZ between 10 and 6.2 ka might have reduced the large-scale production of N_2O in the Arabian Sea and ETSP, significantly contributing to the formation of the N_2O minimum between 8.8 and 6.2 ka.

We also compared the individual responses of terrestrial (temperature and precipitation changes) and marine (denitrification and OMZ changes) proxies from major N_2O -producing regions during 8.8–6.2 ka minimum. For this purpose, we calculated the average Z-score of each record for the period between 8.8 and 6.2 ka and the rest of the Holocene (see Supporting Information S1 for more details on the calculation of the Z-scores) (Figures S8–S12 in Supporting Information S1). The paleo-proxy record illustrates wet and warm conditions around the Asian Monsoon region between 8.8 and 6.2 ka (Berkelhammer et al., 2012; Dykoski et al., 2005; Fleitmann et al., 2007; Hu et al., 2008) (Figure S8 in Supporting Information S1). In contrast, South America experienced dry conditions during the same period (Bird et al., 2011; Van Breukelen et al., 2008; Wang et al., 2007) (Figure 6 and Figure S8 in Supporting Information S1). The average Z-score of $\delta^{15}\text{N}$ records from both ETSP and AS indicates the prolonged weakening of OMZ and reduced N_2O production in both regions during 8.8–6.2 ka (Figure S11 in Supporting Information S1). Hence, the N_2O minimum between 8.8 and 6.2 ka mainly correlates with the prominent decrease in marine N_2O production around the upwelling centers. These results corroborate the findings of Fischer et al. (2019), suggesting a gradual decrease of F_{ocean} by $\sim 1 \text{ TgNyr}^{-1}$, whereas the F_{land} shows a secular trend between 10 and 6 ka (Figures 4 and 5). All these observations suggest that the notable decrease in atmosphere concentration between 10.0 and 6.2 ka is attributed to the significant drop in emission from the marine N_2O sources.

5.3. 6.2–2.2 ka

Between 6.2 and 3.0 ka, the N_2O composite shows a progressive increase ($\sim 12 \text{ ppb}$ or $\sim 0.5 \text{ TgNyr}^{-1}$), which is followed by another N_2O maximum at 3.0–2.2 ka. The N_2O increase correlates with the intensification of Southern Hemisphere monsoons (South American and Australian-Indonesian) whereas the Asian and N. African monsoons show a weakening trend between 6.2 and 2.2 ka (Tables 1 and 2). The contemporary increase in the pre-industrial atmospheric CH_4 is also attributed to the increase in the emissions from the Southern Hemisphere (Beck

Figure 4. Comparison of our N_2O composite and isotope-based terrestrial N_2O flux (F_{Land}) (Fischer et al., 2019) with the terrestrial temperature and precipitation records ($\delta^{18}\text{O}$ of cave deposits) of major monsoon regions of the world: (Top to Bottom) Simulated temperature anomaly of South China (Shi et al., 2021); Dongge Cave, China (Dykoski et al., 2005); Pink Panther Cave, USA (Asmerom et al., 2007); Laguna Pumacocha, Peru (Bird et al., 2011); Cold Air Cave, South Africa (Holmgren et al., 2003); Liang Luar Cave, Indonesia (Griffiths et al., 2009). The black curves over Dongge Cave and Laguna Pumacocha represent the summer insolation (W/m^2) of the Northern and Southern Hemispheres at 15° (Berger & Loutre, 1991). It should be noted that the N_2O composite and F_{Land} are synchronized with WD2014 and AICC2012 gas-age scales respectively.

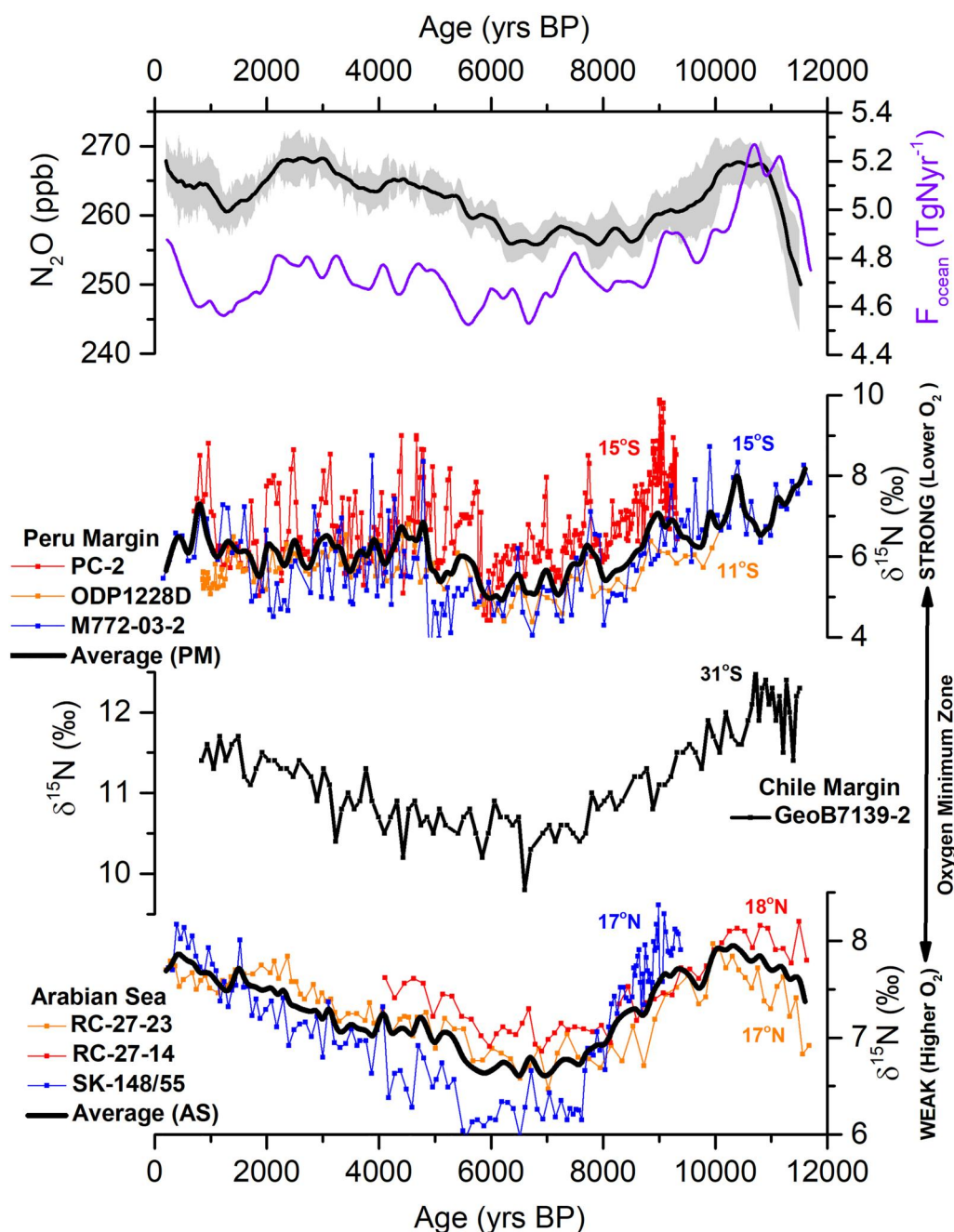


Figure 5. Comparison of N_2O composite and isotope-based marine N_2O flux (F_{ocean}) (Fischer et al., 2019) with the marine sediment $\delta^{15}\text{N}$ records around Eastern Tropical South Pacific sites PC-2 (Agnihotri et al., 2006); M772-003 (Mollier-Vogel et al., 2019), ODP1228D (Agnihotri et al., 2006), GeoB7139-2 (De-Pol-Holz et al., 2007), and Arabian Sea sites RC2714, RC-2723 (Altabet et al., 2002) and SK-148/55 (Kessarkar et al., 2018). It should be noted that the N_2O composite and F_{ocean} are synchronized with WD2014 and AICC2012 gas-age scales respectively.

et al., 2018; Singrayer et al., 2011). In the marine records, the AS and ETSP show a gradual increase in the denitrification process between 6.2 and 2.2 ka, indicating the intensification of OMZ, promotion of N_2O production, and outgassing from those regions (Agnihotri et al., 2006; Altabet et al., 2002; Azharuddin et al., 2022; De-Pol-Holz et al., 2007; Mollier-Vogel et al., 2019). The correlation results also suggest that the N_2O trend during that period corresponds to the intensification in Southern Hemisphere Monsoons and OMZs in AS and ETSP.

Table 1

Correlation Coefficients of N_2O Composite With the N_2O Emission Strength Inferred From Global Paleo-Proxy Records During Four Major Periods of N_2O Variation Discussed in the Present Study

Region/Site (proxy)	11.5–10.0 ka	10.0–6.2 ka	6.2–2.2 ka	2.2–1.4 ka
	Significance level r (lag) $p < 0.05$	Significance level r (lag) $p < 0.05$	Significance level r (lag) $p < 0.05$	Significance level r (lag) $p < 0.05$
Chile Margin ($\delta^{15}N$ Bulk Sediment)	0.32 (200 yrs)	0.85 (–150 yrs)	0.71 (–180 yrs)	0.56 (150 yrs)
Peru Margin ($\delta^{15}N$ Bulk Sediment)	–0.44 (90 yrs)	0.74 (30 yrs)	0.63 (160 yrs)	0.56 (200 yrs)
Arabian Sea ($\delta^{15}N$ Bulk Sediment)	0.78 (–50 yrs)	0.87 (–20 yrs)	0.89 (–150 yrs)	–0.87 (–190 yrs)
Asian Monsoon ($\delta^{18}O$ Stalagmite)	–0.70 (No Lag)	Insignificant correlation	0.86 (–100 yrs)	–0.63 (–10 yrs)
N. American Monsoon ($\delta^{18}O$ Stalagmite)	–0.67 (100 yrs)	–0.35 (200 yrs)	Insignificant correlation	0.68 (180 yrs)
N. African Monsoon ($\delta^{18}O$ Stalagmite)	–0.94 (–70 yrs)	Insignificant correlation	0.48 (–200 yrs)	0.90 (–200 yrs)
S. American Monsoon ($\delta^{18}O$ Stalagmite)	Insignificant correlation	0.86 (190 yrs)	–0.87 (160 yrs)	Insignificant correlation
S. African Monsoon ($\delta^{18}O$ Stalagmite)	Insignificant correlation	0.69 (–10 yrs)	Insignificant correlation	0.31 (–70 yrs)
Australian-Indonesian Monsoon ($\delta^{18}O$ Stalagmite)	–0.72 (–200 yrs)	0.85 (No lag)	–0.44 (–200 yrs)	–0.71 (–180 yrs)

Note. The $\delta^{18}O$ shows a negative correlation with N_2O in case of increased rainfall whereas the $\delta^{15}N$ shows a positive correlation with N_2O in case of increased denitrification.

5.4. 2.2–1.4 ka

The N_2O record shows a prominent 8 ppb ($\sim 0.3 \text{ TgNyr}^{-1}$) decrease between 2.2 ka and 1.4 ka, leading to an N_2O minimum at around 1.4 ka. During the same period, the Asian and Australian-Indonesian monsoons show weakening (Tables 1 and 2). On the other hand, the $\delta^{15}N$ of bulk sediment at Peru Margin sites PC-2 and M772-03 shows a $\sim 2\text{‰}$ decrease indicating the weakened OMZ in the region (Agnihotri et al., 2006; Mollier-Vogel et al., 2019). At the same time, both F_{land} & F_{ocean} show a notable decrease in emissions centering around 1.4 ka (Fischer et al., 2019) (Figures 4 and 5). The N_2O minimum at 1.4 ka ($\sim 600 \text{ CE}$) was previously reported from Styx and NEEM ice core sites and was attributed to the changes in tropical hydroclimate and ocean productivity (Ryu et al., 2020).

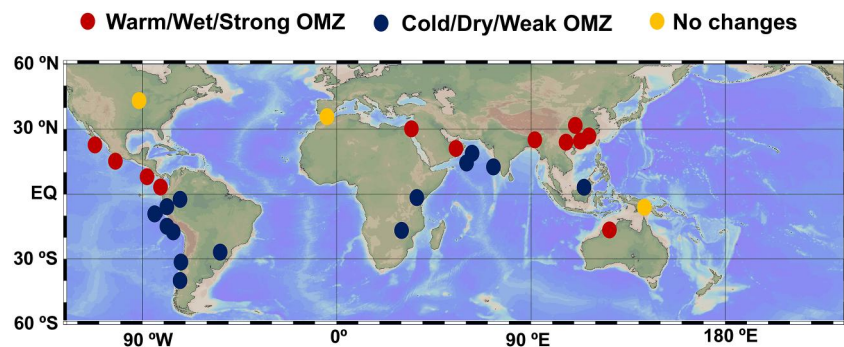


Figure 6. Variation in the marine and terrestrial proxies during N_2O local minimum around 8.8 to 6.2 ka (See Supporting Information S1 for more details). Map source: Ocean Data View (<https://odv.awi.de/>).

Table 2

Plausible Changes (Strengthening (Red)/Weakening (Blue)) in Terrestrial and Marine Sources of N₂O During Each Studied Period

Period (N ₂ O change)	Terrestrial source	Marine source
11.5–10.0 ka (N ₂ O ↑)	Northern Hemisphere Monsoons (Asian, N. African and N. American Monsoons); and Australian-Indonesian Monsoons	Intensified OMZ around Arabian Sea and Chile Margin
10.0–6.2 ka (N ₂ O ↓)	S. American Monsoon	OMZs around the Arabian Sea and Eastern Tropical South Pacific (both Peru and Chile Margins)
6.2–2.2 ka (N ₂ O ↑)	S. American and Australian-Indonesian Monsoons	OMZs around the Arabian Sea and Eastern Tropical South Pacific (both Peru and Chile Margin)
2.2–1.4 ka (N ₂ O ↓)	Asian and Australian-Indonesian Monsoons	OMZ around Eastern Tropical South Pacific (both Peru and Chile Margins)

6. Conclusions

We present the millennial-scale N₂O variation during the Holocene epoch obtained from the SPICE core. The results demonstrate agreement with other existing ice core records from Antarctica and Greenland on a millennial scale. Furthermore, the new high-resolution record from SPICE shows a centennial-scale N₂O minimum around 2.8 ka which is not observed in other ice core records possibly due to lower sample resolution and/or higher age smoothing. We prepared a Holocene N₂O composite by combining the new SPICE results with the existing N₂O records. Our N₂O composite exhibits four distinct periods of N₂O variation consisting of two N₂O maxima during 11–10 ka and 3.0–2.2 ka, followed by two minima during 8.8–6.2 ka and at around 1.4 ka, respectively. The most significant N₂O increase (~15 ppb or ~0.8 TgNyr⁻¹) is observed between 11.5 and 10.0 ka, which corresponds to the increased precipitation around major monsoon regions and intensified the Arabian Sea and Chile Margin OMZ. Subsequently, the ~0.5 TgNyr⁻¹ decrease in N₂O flux between 10.0 and 6.2 ka may plausibly be associated with the reduced N₂O emission owing to aridification in the South American monsoon region and weakening of the Arabian Sea and ETSP OMZ. Between 6.2 and 2.2 ka, the progressive increase (~12 ppb or ~0.5 TgNyr⁻¹) in atmospheric N₂O leading to another N₂O maximum from 3.0 to 2.2 ka are associated with the high N₂O emissions owing to increased precipitation of Southern Hemisphere monsoons and intensified OMZ conditions around the ETSP and the Arabian Sea. Another significant N₂O decrease at 1.4 ka is attributed to the decrease in Northern Hemisphere temperature, reduced precipitation in Asian and Indonesian-Australian monsoon regions, and weakened OMZ around ETSP. Scenario-based numerical modeling studies are required to better understand the relationship between climate and N₂O variation during the Holocene. In addition, the high-resolution study of N₂O isotopologues (δ¹⁵N, δ¹⁸O, and site preference of N₂O molecules) focusing on the Holocene epoch may further help resolve the individual contribution of marine and terrestrial sources and their variation during N₂O maxima and minima.

Data Availability Statement

All data presented in this study are provided in Supplement tables and are available in the PANGAEA cryosphere database which can be accessed using the following links: <https://doi.org/10.1594/PANGAEA.964081> (Azharuddin et al., 2023a); <https://doi.org/10.1594/PANGAEA.964085> (Azharuddin et al., 2023b).

Acknowledgments

We thank the South Pole Ice Core (SPICE) Project and Oregon State University for providing ice samples. Financial support was provided by the National Research Foundation of Korea (NRF) (NRF-2018R1A2B3003256; RS-2023-00278926; RS-2023-00291696). This study was also supported by a research grant (PE24100) from the Korea Polar Research Institute.

References

- Agnihotri, R., Altabet, M. A., & Herbert, T. D. (2006). Influence of marine denitrification on atmospheric N₂O variability during the Holocene. *Geophysical Research Letters*, 33(13), L13704. <https://doi.org/10.1029/2006gl025864>
- Altabet, M. A., Higginson, M. J., & Murray, D. W. (2002). The effect of millennial-scale changes in Arabian Sea denitrification on atmospheric CO₂. *Nature*, 415(6868), 159–162. <https://doi.org/10.1038/415159a>
- Arevalo-Martínez, D. L., Kock, A., Löscher, C. R., Schmitz, R. A., & Bange, H. W. (2015). Massive nitrous oxide emissions from the tropical South Pacific Ocean. *Nature Geoscience*, 8(7), 530–533. <https://doi.org/10.1038/ngeo2469>
- Asmerom, Y., Polyak, V., Burns, S., & Rasmussen, J. (2007). Solar forcing of Holocene climate: New insights from a speleothem record, southwestern United States. *Geology*, 35(1), 1–4. <https://doi.org/10.1130/g22865a.1>
- Azharuddin, S., Ahn, J., Ryu, Y., Brook, E. J., & Salehnia, N. (2023a). Nitrous oxide concentration from South Pole Ice (SPICE) core for the last 11 thousand years. *PANGAEA*. <https://doi.org/10.1594/PANGAEA.964081>

- Azharuddin, S., Ahn, J., Ryu, Y., Brook, E. J., & Salehnia, N. (2023b). Holocene total nitrous oxide flux based on the composite nitrous oxide concentration data. *PANGAEA*. <https://doi.org/10.1594/PANGAEA.964085>
- Azharuddin, S., Govil, P., Singh, A. D., Mishra, R., & Agrawal, S. (2022). Mid-Holocene intensification of the oxygen minimum zone in the northeastern Arabian Sea. *Journal of Asian Earth Sciences*, 227, 105094. <https://doi.org/10.1016/j.jseas.2022.105094>
- Babbin, A. R., Bianchi, D., Jayakumar, A., & Ward, B. B. (2015). Rapid nitrous oxide cycling in the Suboxic Ocean. *Science*, 348(6239), 1127–1129. <https://doi.org/10.1126/science.aaa8380>
- Bai, E., Li, S., Xu, W., Li, W., Dai, W., & Jiang, P. (2013). A meta-analysis of experimental warming effects on terrestrial nitrogen pools and dynamics. *New Phytologist*, 199(2), 441–451. <https://doi.org/10.1111/nph.12252>
- Bar-Matthews, M., & Ayalon, A. (2011). Mid-Holocene climate variations revealed by high-resolution speleothem records from Soreq Cave, Israel and their correlation with cultural changes. *The Holocene*, 21(1), 163–171. <https://doi.org/10.1177/0959683610384165>
- Battaglia, G., & Joos, F. (2018). Marine N₂O emissions from nitrification and denitrification constrained by modern observations and projected in multimillennial global warming simulations. *Global Biogeochemical Cycles*, 32(1), 92–121. <https://doi.org/10.1002/2017gb005671>
- Battle, M., Bender, M., Sowers, T., Tans, P. P., Butler, J. H., Elkins, J. W., et al. (1996). Atmospheric gas concentrations over the past century measured in air from firn at the South Pole. *Nature*, 383(6597), 231–235. <https://doi.org/10.1038/383231a0>
- Beck, J., Bock, M., Schmitt, J., Seth, B., Blunier, T., & Fischer, H. (2018). Bipolar carbon and hydrogen isotope constraints on the Holocene methane budget. *Biogeosciences*, 15(23), 7155–7175. <https://doi.org/10.5194/bg-15-7155-2018>
- Bender, M. L., Floch, G., Chappellaz, J., Suwa, M., Barnola, J. M., Blunier, T., et al. (2006). Gas age–ice age differences and the chronology of the Vostok ice core, 0–100 ka. *Journal of Geophysical Research*, 111(D21), D21115. <https://doi.org/10.1029/2005jd006488>
- Berger, A., & Loutre, M. F. (1991). Insolation values for the climate of the last 10 million years. *Quaternary Science Reviews*, 10(4), 297–317. [https://doi.org/10.1016/0277-3791\(91\)90033-q](https://doi.org/10.1016/0277-3791(91)90033-q)
- Berkehammer, M., Sinha, A., Stott, L., Cheng, H., Pausata, F. S., & Yoshimura, K. (2012). An abrupt shift in the Indian monsoon 4000 years ago. *Geophysical Monograph Series*, 198, 75–87.
- Bird, B. W., Abbott, M. B., Rodbell, D. T., & Vuille, M. (2011). Holocene tropical South American hydroclimate revealed from a decadal resolved lake sediment $\delta^{18}\text{O}$ record. *Earth and Planetary Science Letters*, 310(3–4), 192–202. <https://doi.org/10.1016/j.epsl.2011.08.040>
- Bouwman, A. F., Boumans, L. J. M., & Batjes, N. H. (2002). Emissions of N₂O and NO from fertilized fields: Summary of available measurement data. *Global Biogeochemical Cycles*, 16(4), 6–16–13. <https://doi.org/10.1029/2001gb001811>
- Brovkin, V., Lorenz, S., Raddatz, T., Ilyina, T., Stemmler, I., Toohey, M., & Claussen, M. (2019). What was the source of the atmospheric CO₂ increase during the Holocene? *Biogeosciences*, 16(13), 2543–2555. <https://doi.org/10.5194/bg-16-2543-2019>
- Buizert, C. (2012). *The influence of firn air transport processes and radiocarbon production on gas records from polar firn and ice*, PhD (p. 175). Faculty of Science, University of Copenhagen.
- Cohen, Y., & Gordon, L. I. (1978). Nitrous oxide in the oxygen minimum of the eastern tropical North Pacific: Evidence for its consumption during denitrification and possible mechanisms for its production. *Deep-Sea Research*, 25(6), 509–524. [https://doi.org/10.1016/0146-6291\(78\)90640-9](https://doi.org/10.1016/0146-6291(78)90640-9)
- Cohen, Y., & Gordon, L. I. (1979). Nitrous oxide production in the ocean. *Journal of Geophysical Research*, 84(C1), 347–353. <https://doi.org/10.1029/jc084i01p00347>
- De Pol-Holz, R., Ulloa, O., Lamy, F., Dezileau, L., Sabatier, P., & Hebbeln, D. (2007). Late Quaternary variability of sedimentary nitrogen isotopes in the eastern South Pacific Ocean. *Paleoceanography*, 22(2), PA2207. <https://doi.org/10.1029/2006pa001308>
- Dykoski, C. A., Edwards, R. L., Cheng, H., Yuan, D., Cai, Y., Zhang, M., et al. (2005). A high-resolution, absolute-dated Holocene and deglacial Asian monsoon record from Dongge Cave, China. *Earth and Planetary Science Letters*, 233(1–2), 71–86. <https://doi.org/10.1016/j.epsl.2005.01.036>
- Epifanio, J. A., Brook, E. J., Buizert, C., Edwards, J. S., Sowers, T. A., Kahle, E. C., et al. (2020). The SP19 chronology for the South Pole ice core—Part 2: Gas chronology, Δ age, and smoothing of atmospheric records. *Climate of the Past*, 16(6), 2431–2444. <https://doi.org/10.5194/cp-16-2431-2020>
- Fischer, H., Schmitt, J., Bock, M., Seth, B., Joos, F., Spahni, R., et al. (2019). N₂O changes from the Last Glacial Maximum to the preindustrial—Part 1: Quantitative reconstruction of terrestrial and marine emissions using N₂O stable isotopes in ice cores. *Biogeosciences*, 16(20), 3997–4021. <https://doi.org/10.5194/bg-16-3997-2019>
- Fleitmann, D., Burns, S. J., Mangini, A., Mudelsee, M., Kramers, J., Villa, I., et al. (2007). Holocene ITCZ and Indian monsoon dynamics recorded in stalagmites from Oman and Yemen (Socotra). *Quaternary Science Reviews*, 26(1–2), 170–188. <https://doi.org/10.1016/j.quascirev.2006.04.012>
- Flückiger, J., Blunier, T., Stauffer, B., Chappellaz, J., Spahni, R., Kawamura, K., et al. (2004). N₂O and CH₄ variations during the last glacial epoch: Insight into global processes. *Global Biogeochemical Cycles*, 18(1), GB1020. <https://doi.org/10.1029/2003gb002122>
- Flückiger, J., Dallenbach, A., Blunier, T., Stauffer, B., Stocker, T. F., Raynaud, D., & Barnola, J. M. (1999). Variations in atmospheric N₂O concentration during abrupt climatic changes. *Science*, 285(5425), 227–230. <https://doi.org/10.1126/science.285.5425.227>
- Flückiger, J., Monnin, E., Stauffer, B., Schwander, J., Stocker, T. F., Chappellaz, J., & Barnola, J. M. (2002). High-resolution Holocene N₂O ice core record and its relationship with CH₄ and CO₂. *Global Biogeochemical Cycles*, 16(1), 10–11. <https://doi.org/10.1029/2001gb001417>
- Frey, C., Bange, H. W., Achterberg, E. P., Jayakumar, A., Löscher, C. R., Arévalo-Martínez, D. L., et al. (2020). Regulation of nitrous oxide production in low-oxygen waters off the coast of Peru. *Biogeosciences*, 17(8), 2263–2287. <https://doi.org/10.5194/bg-17-2263-2020>
- Goodwin, P., Oliver, K. I., & Lenton, T. M. (2011). Observational constraints on the causes of Holocene CO₂ change. *Global Biogeochemical Cycles*, 25(3), GB3011. <https://doi.org/10.1029/2010gb003888>
- Griffiths, M. L., Drysdale, R. N., Gagan, M. K., Zhao, J. X., Ayliffe, L. K., Hellstrom, J. C., et al. (2009). Increasing Australian–Indonesian monsoon rainfall linked to early Holocene sea-level rise. *Nature Geoscience*, 2(9), 636–639. <https://doi.org/10.1038/ngeo605>
- Grubbs, F. E. (1969). Procedures for detecting outlying observations in samples. *Technometrics*, 11(1), 1–21. <https://doi.org/10.1080/00401706.1969.10490657>
- Gruber, N., & Galloway, J. N. (2008). An Earth-system perspective of the global nitrogen cycle. *Nature*, 451(7176), 293–296. <https://doi.org/10.1038/nature06592>
- Henry, L. G., McManus, J. F., Curry, W. B., Roberts, N. L., Piotrowski, A. M., & Keigwin, L. D. (2016). North Atlantic ocean circulation and abrupt climate change during the last glaciation. *Science*, 353(6298), 470–474. <https://doi.org/10.1126/science.aaf5529>
- Holmgren, K., Lee-Thorp, J. A., Cooper, G. R., Lundblad, K., Partridge, T. C., Scott, L., et al. (2003). Persistent millennial-scale climatic variability over the past 25,000 years in Southern Africa. *Quaternary Science Reviews*, 22(21–22), 2311–2326. [https://doi.org/10.1016/s0277-3791\(03\)00204-x](https://doi.org/10.1016/s0277-3791(03)00204-x)
- Hu, C., Henderson, G. M., Huang, J., Chen, Z., & Johnson, K. R. (2008). Report of a three-year monitoring programme at Heshang Cave, Central China. *International Journal of Speleology*, 37(3), 1–151. <https://doi.org/10.5038/1827-806x.37.3.1>

- Ishijima, K., Nakazawa, T., & Aoki, S. (2009). Variations of atmospheric nitrous oxide concentration in the northern and western Pacific. *Tellus B: Chemical and Physical Meteorology*, 61(2), 408–415. <https://doi.org/10.3402/tellusb.v61i2.16839>
- Ishijima, K., Sugawara, S., Kawamura, K., Hashida, G., Morimoto, S., Murayama, S., et al. (2007). Temporal variations of the atmospheric nitrous oxide concentration and its $\delta^{15}\text{N}$ and $\delta^{18}\text{O}$ for the latter half of the 20th century reconstructed from firn air analyses. *Journal of Geophysical Research*, 112(D3), D03305. <https://doi.org/10.1029/2006jd007208>
- Ji, Q., Babbin, A. R., Jayakumar, A., Oleynik, S., & Ward, B. B. (2015). Nitrous oxide production by nitrification and denitrification in the Eastern Tropical South Pacific oxygen minimum zone. *Geophysical Research Letters*, 42(24), 10–755. <https://doi.org/10.1002/2015gl066853>
- Joos, F., Spahni, R., Stocker, B. D., Lienert, S., Müller, J., Fischer, H., et al. (2020). N_2O changes from the Last Glacial Maximum to the preindustrial—Part 2: Terrestrial N_2O emissions and carbon–nitrogen cycle interactions. *Biogeosciences*, 17(13), 3511–3543. <https://doi.org/10.5194/bg-17-3511-2020>
- Kessarkar, P. M., Naqvi, S. W. A., Thamban, M., Fernandes, L. L., Siebert, C., Rao, V. P., et al. (2018). Variations in denitrification and ventilation within the Arabian Sea oxygen minimum zone during the Holocene. *Geochemistry, Geophysics, Geosystems*, 19(7), 2179–2193. <https://doi.org/10.1029/2017gc007286>
- Lee, J. E., Edwards, J. S., Schmitt, J., Fischer, H., Bock, M., & Brook, E. J. (2020). Excess methane in Greenland ice cores associated with high dust concentrations. *Geochimica et Cosmochimica Acta*, 270, 409–430. <https://doi.org/10.1016/j.gca.2019.11.020>
- Lilien, D. A., Fudge, T. J., Koutnik, M. R., Conway, H., Osterberg, E. C., Ferris, D. G., et al. (2018). Holocene ice-flow speedup in the vicinity of the South Pole. *Geophysical Research Letters*, 45(13), 6557–6565. <https://doi.org/10.1029/2018gl078253>
- Liu, X., Dong, Y., Qi, Y., Peng, Q., He, Y., Sun, L., et al. (2015). Response of N_2O emission to water and nitrogen addition in temperate typical steppe soil in Inner Mongolia, China. *Soil and Tillage Research*, 151, 9–17. <https://doi.org/10.1016/j.still.2015.01.008>
- Macfarling Meure, C., Etheridge, D., Trudinger, C., Steele, P., Langenfelds, R., Van Ommen, T., et al. (2006). Law Dome CO_2 , CH_4 and N_2O ice core records extended to 2000 years BP. *Geophysical Research Letters*, 33(14), L14810. <https://doi.org/10.1029/2006gl026152>
- Machida, T., Nakazawa, T., Fujii, Y., Aoki, S., & Watanabe, O. (1995). Increase in the atmospheric nitrous oxide concentration during the last 250 years. *Geophysical Research Letters*, 22(21), 2921–2924. <https://doi.org/10.1029/95gl02822>
- Minschwaner, K., Carver, R. W., Briegleb, B. P., & Roche, A. E. (1998). Infrared radiative forcing and atmospheric lifetimes of trace species based on observations from UAES. *Journal of Geophysical Research*, 103(D18), 23243–23253. <https://doi.org/10.1029/98jd02116>
- Mollier-Vogel, E., Martinez, P., Blanz, T., Robinson, R., Desprat, S., Etourneau, J., et al. (2019). Mid-Holocene deepening of the Southeast Pacific oxycline. *Global and Planetary Change*, 172, 365–373. <https://doi.org/10.1016/j.gloplacha.2018.10.020>
- Mosley-Thompson, E., Paskievitch, J. F., Gow, A. J., & Thompson, L. G. (1999). Late 20th century increase in South Pole snow accumulation. *Journal of Geophysical Research*, 104(D4), 3877–3886. <https://doi.org/10.1029/1998jd200092>
- Naqvi, S. W. A., Jayakumar, D. A., Narvekar, P. V., Naik, H., Sarma, V. V. S. S., D'souza, W., et al. (2000). Increased marine production of N_2O due to intensifying anoxia on the Indian continental shelf. *Nature*, 408(6810), 346–349. <https://doi.org/10.1038/35042551>
- Naqvi, S. W. A., & Noronha, R. J. (1991). Nitrous oxide in the Arabian Sea. *Deep Sea Research Part A: Oceanographic Research Papers*, 38(7), 871–890. [https://doi.org/10.1016/0198-0149\(91\)90023-9](https://doi.org/10.1016/0198-0149(91)90023-9)
- Pedro, J. B., Jochum, M., Buizert, C., He, F., Barker, S., & Rasmussen, S. O. (2018). Beyond the bipolar seesaw: Toward a process understanding of interhemispheric coupling. *Quaternary Science Reviews*, 192, 27–46. <https://doi.org/10.1016/j.quascirev.2018.05.005>
- Philippot, L., Hallin, S., & Schloter, M. (2007). Ecology of denitrifying prokaryotes in agricultural soil. *Advances in Agronomy*, 96, 249–305. [https://doi.org/10.1016/s0065-2113\(07\)96003-4](https://doi.org/10.1016/s0065-2113(07)96003-4)
- Pichevin, L., Bard, E., Martinez, P., & Billy, I. (2007). Evidence of ventilation changes in the Arabian Sea during the late Quaternary: Implication for denitrification and nitrous oxide emission. *Global Biogeochemical Cycles*, 21(4), GB4008. <https://doi.org/10.1029/2006gb002852>
- Potter, C. S., Matson, P. A., Vitousek, P. M., & Davidson, E. A. (1996). Process modeling of controls on nitrogen trace gas emissions from soils worldwide. *Journal of Geophysical Research*, 101(D1), 1361–1377. <https://doi.org/10.1029/95jd02028>
- Prather, M. J., Hsu, J., DeLuca, N. M., Jackman, C. H., Oman, L. D., Douglass, A. R., et al. (2015). Measuring and modeling the lifetime of nitrous oxide including its variability. *Journal of Geophysical Research: Atmospheres*, 120(11), 5693–5705. <https://doi.org/10.1002/2015jd023267>
- Rohde, R. A., Price, P. B., Bay, R. C., & Bramall, N. E. (2008). In situ microbial metabolism as a cause of gas anomalies in ice. *Proceedings of the National Academy of Sciences*, 105(25), 8667–8672. <https://doi.org/10.1073/pnas.0803763105>
- Röthlisberger, R., Hutterli, M. A., Sommer, S., Wolff, E. W., & Mulvaney, R. (2000). Factors controlling nitrate in ice cores: Evidence from the Dome C deep ice core. *Journal of Geophysical Research*, 105(D16), 20565–20572. <https://doi.org/10.1029/2000jd900264>
- Rubino, M., Etheridge, D. M., Thornton, D. P., Howden, R., Allison, C. E., Francey, R. J., et al. (2019). Revised records of atmospheric trace gases CO_2 , CH_4 , N_2O , and $\delta^{13}\text{C-CO}_2$ over the last 2000 years from Law Dome, Antarctica. *Earth System Science Data*, 11(2), 473–492. <https://doi.org/10.5194/essd-11-473-2019>
- Ryu, Y., Ahn, J., & Yang, J. W. (2018). High-precision measurement of N_2O concentration in ice cores. *Environmental Science & Technology*, 52(2), 731–738. <https://doi.org/10.1021/acs.est.7b05250>
- Ryu, Y., Ahn, J., Yang, J. W., Brook, E. J., Timmermann, A., Blunier, T., et al. (2020). Atmospheric nitrous oxide variations on centennial time scales during the past two millennia. *Global Biogeochemical Cycles*, 34(9), e2020GB006568. <https://doi.org/10.1029/2020gb006568>
- Samarkin, V. A., Madigan, M. T., Bowles, M. W., Casciotti, K. L., Priscu, J. C., McKay, C. P., & Joye, S. B. (2010). Abiotic nitrous oxide emission from the hypersaline Don Juan Pond in Antarctica. *Nature Geoscience*, 3(5), 341–344. <https://doi.org/10.1038/ngeo847>
- Schilt, A., Baumgartner, M., Blunier, T., Schwander, J., Spahni, R., Fischer, H., & Stocker, T. F. (2010). Glacial–interglacial and millennial-scale variations in the atmospheric nitrous oxide concentration during the last 800,000 years. *Quaternary Science Reviews*, 29(1–2), 182–192. <https://doi.org/10.1016/j.quascirev.2009.03.011>
- Schilt, A., Baumgartner, M., Eicher, O., Chappellaz, J., Schwander, J., Fischer, H., & Stocker, T. F. (2013). The response of atmospheric nitrous oxide to climate variations during the last glacial period. *Geophysical Research Letters*, 40(9), 1888–1893. <https://doi.org/10.1002/grl.50380>
- Schilt, A., Brook, E. J., Bauska, T. K., Baggenstos, D., Fischer, H., Joos, F., et al. (2014). Isotopic constraints on marine and terrestrial N_2O emissions during the last deglaciation. *Nature*, 516(7530), 234–237. <https://doi.org/10.1038/nature13971>
- Schmittner, A., Galbraith, E. D., Hostetler, S. W., Pedersen, T. F., & Zhang, R. (2007). Large fluctuations of dissolved oxygen in the Indian and Pacific oceans during Dansgaard-Oeschger oscillations caused by variations of North Atlantic Deep Water subduction. *Paleoceanography*, 22(3), PA3207. <https://doi.org/10.1029/2006pa001384>
- Severinghaus, J. P., Grachev, A., & Battle, M. (2001). Thermal fractionation of air in polar firn by seasonal temperature gradients. *Geochemistry, Geophysics, Geosystems*, 2(7), 1048. <https://doi.org/10.1029/2000gc000146>
- Shi, F., Lu, H., Guo, Z., Yin, Q., Wu, H., Xu, C., et al. (2021). The position of the Current Warm Period in the context of the past 22,000 years of summer climate in China. *Geophysical Research Letters*, 48(5), e2020GL091940. <https://doi.org/10.1029/2020gl091940>
- Sigl, M., Fudge, T. J., Winstrup, M., Cole-Dai, J., Ferris, D., McConnell, J. R., et al. (2016). The WAIS Divide deep ice core WD2014 chronology—Part 2: Annual-layer counting (0–31 ka BP). *Climate of the Past*, 12(3), 769–786. <https://doi.org/10.5194/cp-12-769-2016>

- Singarayer, J. S., Valdes, P. J., Friedlingstein, P., Nelson, S., & Beerling, D. J. (2011). Late Holocene methane rise caused by orbitally controlled increase in tropical sources. *Nature*, 470(7332), 82–85. <https://doi.org/10.1038/nature09739>
- Sowers, T. (2001). N₂O record spanning the penultimate deglaciation from the Vostok ice core. *Journal of Geophysical Research*, 106(D23), 31903–31914. <https://doi.org/10.1029/2000jd900707>
- Spahni, R., Chappellaz, J., Stocker, T. F., Loulergue, L., Hausammann, G., Kawamura, K., et al. (2005). Atmospheric methane and nitrous oxide of the late Pleistocene from Antarctic ice cores. *Science*, 310(5752), 1317–1321. <https://doi.org/10.1126/science.1120132>
- Stehfest, E., & Bouwman, L. (2006). N₂O and NO emission from agricultural fields and soils under natural vegetation: Summarizing available measurement data and modeling of global annual emissions. *Nutrient Cycling in Agroecosystems*, 74(3), 207–228. <https://doi.org/10.1007/s10705-006-9000-7>
- Suntharalingam, P., Sarmiento, J. L., & Toggweiler, J. R. (2000). Global significance of nitrous-oxide production and transport from oceanic low-oxygen zones: A modeling study. *Global Biogeochemical Cycles*, 14(4), 1353–1370. <https://doi.org/10.1029/1999gb900100>
- Syakila, A., & Kroeze, C. (2011). The global nitrous oxide budget revisited. *Greenhouse Gas Measurement and Management*, 1(1), 17–26. <https://doi.org/10.3763/ghgmm.2010.0007>
- Tian, H., Xu, R., Canadell, J. G., Thompson, R. L., Winiwarter, W., Suntharalingam, P., et al., (2020). A comprehensive quantification of global nitrous oxide sources and sinks. *Nature*, 586(7828), 248–256. <https://doi.org/10.1038/s41586-020-2780-0>
- Tiano, L., Garcia-Robledo, E., Dalsgaard, T., Devol, A. H., Ward, B. B., Ulloa, O., et al. (2014). Oxygen distribution and aerobic respiration in the north and south eastern tropical Pacific oxygen minimum zones. *Deep Sea Research Part I: Oceanographic Research Papers*, 94, 173–183. <https://doi.org/10.1016/j.dsr.2014.10.001>
- Van Breukelen, M. R., Vonhof, H. B., Hellstrom, J. C., Wester, W. C. G., & Kroon, D. (2008). Fossil dripwater in stalagmites reveals Holocene temperature and rainfall variation in Amazonia. *Earth and Planetary Science Letters*, 275(1–2), 54–60. <https://doi.org/10.1016/j.epsl.2008.07.060>
- Wang, X., Auler, A. S., Edwards, R. L., Cheng, H., Ito, E., Wang, Y., et al. (2007). Millennial-scale precipitation changes in southern Brazil over the past 90,000 years. *Geophysical Research Letters*, 34(23), L23701. <https://doi.org/10.1029/2007gl031149>
- Wang, Y., Guo, J., Vogt, R. D., Mulder, J., Wang, J., & Zhang, X. (2018). Soil pH as the chief modifier for regional nitrous oxide emissions: New evidence and implications for global estimates and mitigation. *Global Change Biology*, 24(2), e617–e626. <https://doi.org/10.1111/gcb.13966>
- Winski, D. A., Fudge, T. J., Ferris, D. G., Osterberg, E. C., Fegyveresi, J. M., Cole-Dai, J., et al. (2019). The SP19 chronology for the South Pole Ice Core—Part 1: Volcanic matching and annual layer counting. *Climate of the Past*, 15(5), 1793–1808. <https://doi.org/10.5194/cp-15-1793-2019>
- Xu, R., Tian, H., Lu, C., Pan, S., Chen, J., Yang, J., & Zhang, B. (2017). Preindustrial nitrous oxide emissions from the land biosphere estimated by using a global biogeochemistry model. *Climate of the Past*, 13(7), 977–990. <https://doi.org/10.5194/cp-13-977-2017>
- Yang, J. W., Ahn, J., Brook, E. J., & Ryu, Y. (2017). Atmospheric methane control mechanisms during the early Holocene. *Climate of the Past*, 13(9), 1227–1242. <https://doi.org/10.5194/cp-13-1227-2017>
- Yang, S., Chang, B. X., Warner, M. J., Weber, T. S., Bourbonnais, A. M., Santoro, A. E., et al. (2020). Global reconstruction reduces the uncertainty of oceanic nitrous oxide emissions and reveals a vigorous seasonal cycle. *Proceedings of the National Academy of Sciences of the United States of America*, 117(22), 11954–11960. <https://doi.org/10.1073/pnas.1921914117>
- Zhang, X., Liu, W., Schloter, M., Zhang, G., Chen, Q., Huang, J., et al. (2013). Response of the abundance of key soil microbial nitrogen-cycling genes to multi-factorial global changes. *PLoS One*, 8(10), e76500. <https://doi.org/10.1371/journal.pone.0076500>
- Zheng, Y., Singarayer, J. S., Cheng, P., Yu, X., Liu, Z., Valdes, P. J., & Pancost, R. D. (2014). Holocene variations in peatland methane cycling associated with the Asian summer monsoon system. *Nature Communications*, 5(1), 4631. <https://doi.org/10.1038/ncomms5631>
- Zhuang, Q., Lu, Y., & Chen, M. (2012). An inventory of global N₂O emissions from the soils of natural terrestrial ecosystems. *Atmospheric Environment*, 47, 66–75. <https://doi.org/10.1016/j.atmosenv.2011.11.036>

References From the Supporting Information

- Arellano-Torres, E., Ganeshram, R. S., Pichevin, L. E., & Salas-de-Leon, D. A. (2015). Persistent millennial-scale climate variability in the eastern tropical North Pacific over the last two glacial cycles. *Paleoceanography*, 30(6), 682–701. <https://doi.org/10.1002/2014pa002714>
- Blunier, T., & Brook, E. J. (2001). Timing of millennial-scale climate change in Antarctica and Greenland during the last glacial period. *Science*, 291(5501), 109–112. <https://doi.org/10.1126/science.291.5501.109>
- Blunier, T., Spahni, R., Barnola, J. M., Chappellaz, J., Loulergue, L., & Schwander, J. (2007). Synchronization of ice core records via atmospheric gases. *Climate of the Past*, 3(2), 325–330. <https://doi.org/10.5194/cp-3-325-2007>
- Conroy, J. L., Overpeck, J. T., Cole, J. E., Shanahan, T. M., & Steinitz-Kannan, M. (2008). Holocene changes in eastern tropical Pacific climate inferred from a Galápagos lake sediment record. *Quaternary Science Reviews*, 27(11–12), 1166–1180. <https://doi.org/10.1016/j.quascirev.2008.02.015>
- Denniston, R. F., González, L. A., Baker, R. G., Asmerom, Y., Reagan, M. K., Edwards, R. L., & Alexander, E. C. (1999). Speleothem evidence for Holocene fluctuations of the prairie-forest ecotone, north-central USA. *The Holocene*, 9(6), 671–676. <https://doi.org/10.1191/095968399674716399>
- Denniston, R. F., Wyrwoll, K. H., Polyak, V. J., Brown, J. R., Asmerom, Y., Wanamaker, A. D., Jr., et al. (2013). A Stalagmite record of Holocene Indonesian–Australian summer monsoon variability from the Australian tropics. *Quaternary Science Reviews*, 78, 155–168. <https://doi.org/10.1016/j.quascirev.2013.08.004>
- Kienast, S. S., Kienast, M., Jaccard, S., Calvert, S. E., & François, R. (2006). Testing the silica leakage hypothesis with sedimentary opal records from the eastern equatorial Pacific over the last 150 kyrs. *Geophysical Research Letters*, 33(15), L15607. <https://doi.org/10.1029/2006gl026651>
- Köhler, P. (2010). Rapid changes in ice core gas records—Part 1: On the accuracy of methane synchronisation of ice cores. *Climate of the Past Discussions*, 6(4), 1453–1471.
- Martinez, P., & Robinson, R. S. (2010). Increase in water column denitrification during the last deglaciation: The influence of oxygen demand in the eastern equatorial Pacific. *Biogeosciences*, 7(1), 1–9. <https://doi.org/10.5194/bg-7-1-2010>
- Montade, V., Peyron, O., Favier, C., Francois, J. P., & Haberle, S. G. (2019). A pollen–climate calibration from western Patagonia for palaeoclimatic reconstructions. *Journal of Quaternary Science*, 34(1), 76–86. <https://doi.org/10.1002/jqs.3082>
- Partin, J. W., Cobb, K. M., Adkins, J. F., Clark, B., & Fernandez, D. P. (2007). Millennial-scale trends in west Pacific warm pool hydrology since the Last Glacial Maximum. *Nature*, 449(7161), 452–455. <https://doi.org/10.1038/nature06164>

- Pichevin, L. E., Ganeshram, R. S., Francavilla, S., Arellano-Torres, E., Pedersen, T. F., & Beaufort, L. (2010). Interhemispheric leakage of isotopically heavy nitrate in the eastern tropical Pacific during the last glacial period. *Paleoceanography*, 25, PA1204. <https://doi.org/10.1029/2009pa001754>
- Salvattei, R., Schneider, R. R., Blanz, T., & Mollier-Vogel, E. (2019). Deglacial to Holocene ocean temperatures in the Humboldt Current System as indicated by alkenone paleothermometry. *Geophysical Research Letters*, 46(1), 281–292. <https://doi.org/10.1029/2018gl080634>
- Veres, D., Bazin, L., Landais, A., Toyé Mahamadou Kele, H., Lemieux-Dudon, B., Parrenin, F., et al. (2013). The Antarctic ice core chronology (AICC2012): An optimized multi-parameter and multi-site dating approach for the last 120 thousand years. *Climate of the Past*, 9(4), 1733–1748. <https://doi.org/10.5194/cp-9-1733-2013>
- Verschuren, D., Olago, D. O., Rucina, S. M., Odhengo, P. O., & ICDP DeepCHALLA Consortium (2013). DeepCHALLA: Two glacial cycles of climate and ecosystem dynamics from equatorial East Africa. *Scientific Drilling*, 15, 72–76. <https://doi.org/10.5194/sd-15-72-2013>
- Wassenburg, J. A., Dietrich, S., Fietzke, J., Fohlmeister, J., Jochum, K. P., Scholz, D., et al. (2016). Reorganization of the North Atlantic Oscillation during early Holocene deglaciation. *Nature Geoscience*, 9(8), 602–605. <https://doi.org/10.1038/ngeo2767>
- Verschuren, D., Sinninghe Damsté, J. S., Moernaut, J., Kristen, I., Blaauw, M., Fagot, M., & Haug, G. H. (2009). Half-precessional dynamics of monsoon rainfall near the East African Equator. *Nature*, 462(7273), 637–641. <https://doi.org/10.1038/nature08520>